

Coexistence of multiple regimes for near-field thermal radiation between two layers supporting surface phonon polaritons in the infrared

Mathieu Francoeur,^{1,*} M. Pinar Mengüç,² and Rodolphe Vaillon³

¹*Radiative Energy Transfer Laboratory, Department of Mechanical Engineering, University of Utah, Salt Lake City, Utah 84112, USA*

²*Ozyegin University, Altunizade, Uskudar, 34662 Istanbul, Turkey*

³*Université de Lyon, CNRS, INSA-Lyon, UCBL, CETHIL, UMR5008, F-69621, Villeurbanne, France*

(Received 25 January 2011; revised manuscript received 14 June 2011; published 8 August 2011)

We demonstrate the coexistence of different near-field thermal radiation regimes between two layers supporting surface phonon polaritons (SPhPs) in the infrared. These regimes exist when the distance of separation between the media d is much smaller than the dominant emission wavelength. This coexistence is noticed after computations of the near-field radiative heat transfer coefficient h_r for silicon carbide films using fluctuational electrodynamics and following an asymptotic analysis of h_r . We show that the emergence of these regimes is a function of a dimensionless variable D defined as the ratio of the layer thickness t to d . When $D \gg 1$ for both films, SPhPs dominating near-field radiant energy exchange do not couple within the layers, such that h_r follows a d^{-2} power law as for the case of two planar half-spaces. When $D \ll 1$ for both layers, the dominant SPhPs couple within the films, thus resulting in a splitting of the spectral distribution of flux into two distinct modes. Despite this splitting, the asymptotic expansion reveals that h_r varies as d^{-2} due to the fact that the spectral bands of high emission and absorption are essentially the same for both films. However, when both layers have a thickness of the order of a nanometer or less, a purely theoretical regime emerges where h_r follows a d^{-4} asymptote. Also, when one layer has $D \ll 1$ while the other one is characterized by $D \gg 1$, there is an important mismatch between the spectral bands of high emission and absorption of the films, thus resulting in a h_r varying as d^{-3} . These various near-field thermal radiation regimes are finally summarized in a comprehensive regime map. This map provides a clear understanding of near-field thermal radiation regimes between two layers, which are particularly important for designing highly efficient nanoscale-gap thermophotovoltaic power generation devices.

DOI: [10.1103/PhysRevB.84.075436](https://doi.org/10.1103/PhysRevB.84.075436)

PACS number(s): 73.20.Mf, 78.66.-w, 44.40.+a, 42.25.Bs

I. INTRODUCTION

It is well-known that radiation heat transfer between bodies separated by a distance d less than the dominant wavelength emitted λ_w can exceed the blackbody predictions due to the contribution from evanescent waves.¹⁻⁷ In the case involving two planar half-spaces (i.e., bulk materials) supporting surface phonon polaritons (SPhPs) in the infrared, the near-field radiative heat flux varies as d^{-2} when $d \ll \lambda_w$.³ If the media exchanging thermal radiation are thin films supporting SPhPs, with thicknesses less than λ_w , the situation becomes more complex as these resonant electromagnetic surface waves can couple within the layers, thus affecting the spectral distribution of the radiant energy transferred.⁸⁻¹⁰ SPhP mediated near-field heat transfer between bulks has also been analyzed experimentally by different groups.¹¹⁻¹³

Near-field thermal radiation involving thin films has recently drawn considerable attention in the literature,^{8-10,14-20} such that it is crucial to define in a clear manner the different regimes involved when two layers are exchanging radiative energy. From an engineering point of view, thin films supporting SPhPs in the infrared could play a key role in designing low operating temperature nanoscale gap thermophotovoltaic (nano-TPV) energy conversion devices.²¹⁻²⁵ We have shown in Ref. 25 that a nano-TPV system involving a bulk radiator at high temperature (~ 1000 – 2000 K), as proposed previously in the literature,²²⁻²⁴ would suffer from extremely low conversion efficiency due to an overheating of the cell converting thermal radiation into electricity. Thin films supporting SPhPs in the infrared could potentially be employed

for low operating temperature radiators (~ 300 – 400 K) in order to selectively transfer near-field thermal radiation toward a low band-gap cell. Such engineering design obviously requires a fundamental understanding of the underlying physics of near-field radiation transfer between layers supporting SPhPs.

Ben-Abdallah *et al.*¹⁹ reported that the radiative heat transfer coefficient h_r between two silicon carbide (SiC) films varies as d^{-2} when both layers have the same thickness, while they observed a d^{-3} regime when the symmetry between the film thicknesses is broken. In this paper, we show and discuss the physics behind the coexistence of d^{-2} , d^{-3} , and d^{-4} regimes of near-field thermal radiation between two layers supporting SPhPs in the infrared. We demonstrate that the emergence of these regimes is not only function of the thickness of the layers but also depends strongly on the separation gap d . This conclusion is reached by calculating the total (i.e., spectrally integrated) radiative heat transfer coefficient h_r and then following an asymptotic analysis of the analytical expression for h_r .

The paper is structured as follows. An analytical expression for the near-field radiative heat transfer coefficient h_r between two films is first derived. Then, numerical calculations of h_r , as a function of d for SiC involving different film thicknesses, are provided and analyzed. An asymptotic expansion of the radiative heat transfer coefficient is performed in the fourth section to determine the conditions for which the different regimes are obtained, and the results are summarized in a comprehensive regime map. Concluding remarks are finally given.

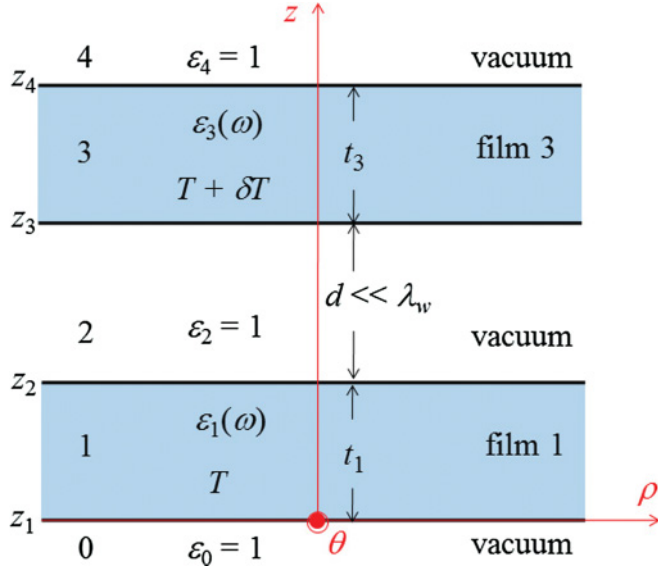


FIG. 1. (Color online) Schematic representation of the geometry considered: two films of thicknesses t_1 and t_3 are separated by a vacuum gap d .

II. NEAR-FIELD RADIATIVE HEAT TRANSFER COEFFICIENT BETWEEN TWO FILMS

We consider the problem shown in Fig. 1, where two layers of thicknesses t_1 and t_3 are surrounded by a vacuum and separated by a gap $d \ll \lambda_w$. It is also assumed that the media, with perfectly smooth and parallel surfaces, are in local thermodynamic equilibrium, homogeneous, nonmagnetic, and described by a dielectric function $\varepsilon(\omega)$ local in space. Only the variations along the z -direction are considered, as the system is azimuthally symmetric and infinite in the ρ -direction.

The total net radiative heat flux (including contributions from both propagating and evanescent waves) exchanged by the layers is calculated as follows:

$$q_{\text{net}} = [q_{13}(z_3^+) - q_{14}(z_4^+)] - [q_{31}(z_2^-) - q_{30}(z_1^-)], \quad (1)$$

where q_{ml} implies a flux emitted by medium m and calculated in layer l . The first term in square brackets in Eq. (1) represents the flux absorbed by layer 3 due to the emitting film 1, and the second term in square brackets is the flux absorbed by layer 1 due to emission from film 3. Near-field radiative heat transfer is analyzed using the fluctuational electrodynamics formalism, where a stochastic current density term is added into the Maxwell equations to model thermal radiation emission.²⁶ The net radiative heat flux exchanged between the layers is calculated by computing the z -component of the Poynting vector at the locations z_j^{\pm} as specified in Eq. (1) and by applying the fluctuation-dissipation theorem²⁶ along with substituting the appropriate components of the dyadic Green's functions for one-dimensional layered media.²⁷ In this work, it is assumed that medium 1 is at temperature T , while layer 3 is at temperature $T + \delta T$, such that the radiative heat transfer coefficient h_r , defined as the net radiative flux divided by δT as $\delta T \rightarrow 0$, is calculated.²⁸ Starting with the analytical expression

for the near-field radiative heat flux between two films,⁹ h_r can be written as

$$h_r = \frac{1}{\pi^2} \int_0^\infty d\omega \frac{\partial \Theta(\omega, T)}{\partial T} \sum_{\gamma=TE, TM} \left[\int_0^{k_v} k_\rho dk_\rho \times \frac{(1 - |R_1^\gamma|^2 - |T_1^\gamma|^2)(1 - |R_3^\gamma|^2 - |T_3^\gamma|^2)}{4 |1 - R_1^\gamma R_3^\gamma e^{2ik_z d}|^2} + \int_{k_v}^\infty k_\rho dk_\rho e^{2ik_z d} \frac{\text{Im}(R_1^\gamma) \text{Im}(R_3^\gamma)}{|1 - R_1^\gamma R_3^\gamma e^{2ik_z d}|^2} \right], \quad (2)$$

where k_ρ is the wave vector parallel to the surfaces of the layers, k_{zj} is the z -component of the wave vector in medium j , and k_v is the magnitude of the wave vector in vacuum. T_j^γ and R_j^γ are the transmission and reflection coefficients of layer j , respectively, in polarization state γ . They are given as $T_j^\gamma = (t_{j-1,j}^\gamma t_{j,j+1}^\gamma e^{ik_{zj} t_j}) / (1 + r_{j-1,j}^\gamma r_{j,j+1}^\gamma e^{2ik_{zj} t_j})$ and $R_j^\gamma = (r_{j-1,j}^\gamma + r_{j,j+1}^\gamma e^{2ik_{zj} t_j}) / (1 + r_{j-1,j}^\gamma r_{j,j+1}^\gamma e^{2ik_{zj} t_j})$, where $t_{j,j+1}^\gamma$ and $r_{j,j+1}^\gamma$ are respectively the Fresnel transmission and reflection coefficients at the interface delimiting media j and $j + 1$. The term $\partial \Theta(\omega, T) / \partial T$ is the derivative of the mean energy of an electromagnetic state with respect to the temperature and is given by $\hbar^2 \omega^2 e^{\hbar\omega/k_b T} / k_b T^2 (e^{\hbar\omega/k_b T} - 1)^2$.

III. CALCULATION OF THE NEAR-FIELD RADIATIVE HEAT TRANSFER COEFFICIENT FOR SILICON CARBIDE

In this section, the near-field radiative heat transfer coefficient given by Eq. (2) is calculated and reported as a function of the vacuum gap for various film thicknesses. The dielectric function of SiC is modeled assuming a Lorentz oscillator:²⁹ $\varepsilon(\omega) = \varepsilon_\infty (\omega^2 - \omega_{LO}^2 + i\Gamma\omega) / (\omega^2 - \omega_{TO}^2 + i\Gamma\omega)$, where $\varepsilon_\infty = 6.7$, $\omega_{TO} = 1.494 \times 10^{14}$ rad/s, $\omega_{LO} = 1.825 \times 10^{14}$ rad/s, and $\Gamma = 8.966 \times 10^{11}$ s⁻¹. First, h_r profiles are shown in Figs. 2(a) and 2(b) as a function of d (from 1 to 100 nm) for $T = 300$ K and by assuming that medium 3 is a bulk (i.e., $t_3 \rightarrow \infty$), while $t_1 = 1, 5, 10$, and 50 nm.

The results of Fig. 2(a) suggest that both d^{-2} and d^{-3} regimes coexist between a film and a bulk, as clearly depicted in Fig. 2(b) for $t_1 = 10$ nm. Hereafter, we use the dimensionless ratio $D_j = t_j/d$, where $D_3 \gg 1$ for all d in Figs. 2(a) and 2(b). In Fig. 2(b), for d smaller than 10 nm, where $D_1 \gg 1$, h_r varies as d^{-2} , while for d larger than 10 nm where $D_1 \ll 1$, h_r varies as d^{-3} . Around a 10-nm-thick gap, there is a region of transition between the d^{-2} and d^{-3} regimes; in this zone, h_r can slightly exceed the values predicted between two bulks, as shown in Fig. 2(a) and discussed in Ref. 16. For the limiting case of two bulks, both D_1 and $D_3 \gg 1$ for all d , thus resulting in a h_r following a d^{-2} power law. Conversely, for the limiting case of a 1-nm-thick film, D_1 is never greater than unity for the d considered in Fig. 2(a), such that h_r varies strictly as d^{-3} .

Figure 3(a) shows h_r curves as a function of d , but this time both media 1 and 3 are of finite thickness; the results are compared with h_r for two bulk materials. In Fig. 3(b), the case where $t_1 = 50$ nm and $t_3 = 10$ nm is analyzed more closely.

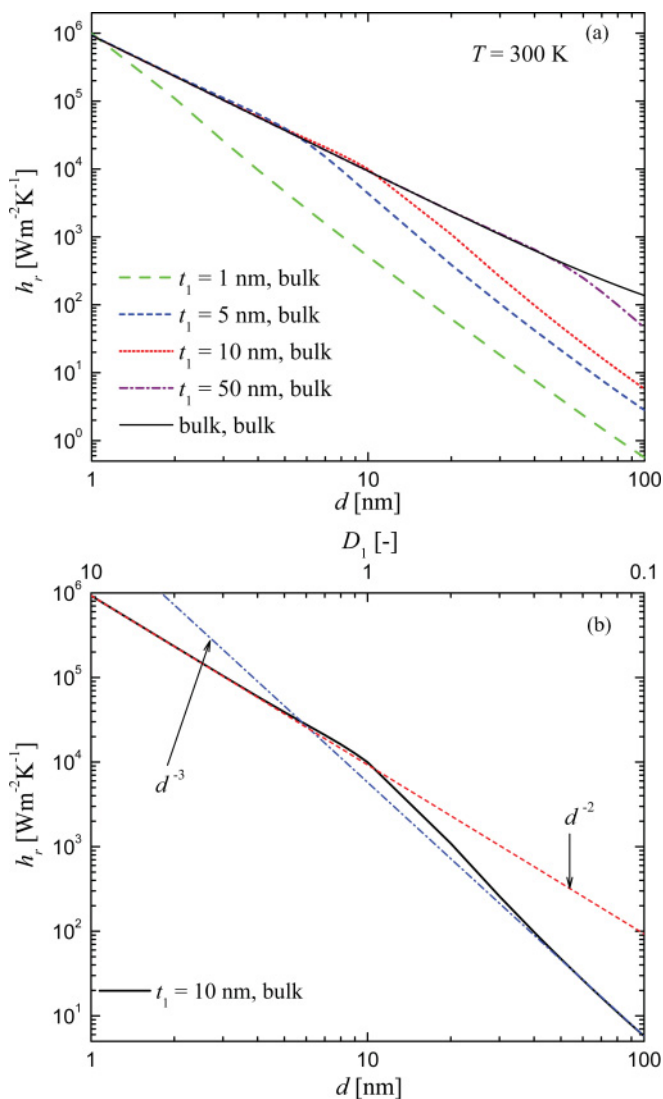


FIG. 2. (Color online) (a) Radiative heat transfer coefficient h_r as a function of d for $t_1 = 1, 5, 10,$ and 50 nm and $t_3 \rightarrow \infty$ (bulk); results are compared with h_r between two bulks. (b) Identification of the d^{-2} and d^{-3} regimes for $t_1 = 10$ nm. The temperature T for all simulations is fixed at 300 K.

It was concluded in Ref. 19 that h_r varies as d^{-3} when the films do not have the same thickness. Clearly, by inspecting Figs. 2 and 3, we see that this is not the case. In Fig. 3(b) where $t_1 = 50$ nm and $t_3 = 10$ nm, both D_1 and $D_3 \gg 1$ for a 1-nm-thick gap. Accordingly, h_r follows a d^{-2} power law up to $d \approx 7$ nm; above this threshold, the criterion $D_3 \gg 1$ becomes questionable. For a 100-nm-thick vacuum gap, $D_1 < 1$, while it is reasonable to assume that $D_3 \ll 1$. Consequently, the d^{-2} regime starts re-emerging for d slightly less than 100 nm. The analysis of the region connecting these two d^{-2} regimes is somehow more complex. For d between 10 and 50 nm, $D_1 \gg 1$ when $D_3 < 1$ while $D_1 > 1$ when it is reasonable to assume that $D_3 \ll 1$. Therefore, the h_r curve within that transition region is lying around a d^{-3} power law without completely reaching it as in Figs. 2(a) and 2(b), since a fully developed d^{-3} regime requires $D_1 \gg 1$ and $D_3 \ll 1$ (or vice versa).

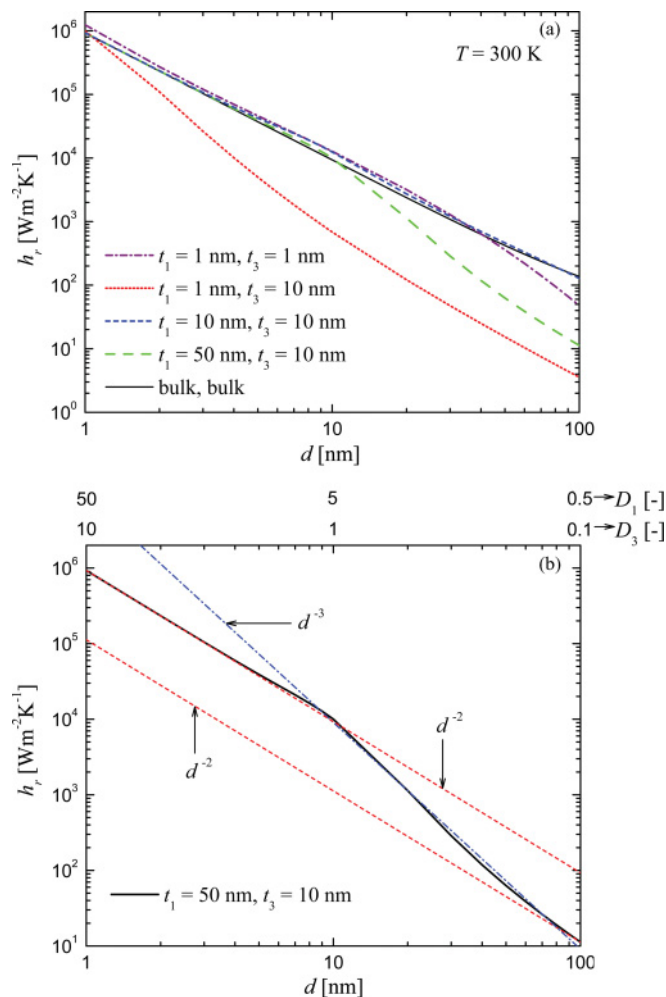


FIG. 3. (Color online) (a) Radiative heat transfer coefficient h_r as a function of d for $t_1 = t_3 = 1$ nm, $t_1 = 1$ nm, $t_3 = 10$ nm, $t_1 = t_3 = 10$ nm, and $t_1 = 50$ nm, $t_3 = 10$ nm; results are compared with h_r between two bulks. (b) Identification of the d^{-2} and d^{-3} regimes for $t_1 = 50$ nm and $t_3 = 10$ nm. The temperature T for all simulations is fixed at 300 K.

At first glance, the results for films of equal thickness seem to be in correct agreement with the observations made in Ref. 19. Inspection of Fig. 3(a) for $t_1 = t_3 = 1$ nm and $t_1 = t_3 = 10$ nm reveals, however, that there is a transition region around a D value of unity, connecting two d^{-2} regimes, where h_r slightly exceeds the values predicted for two bulks. Moreover, when both layers are 1 nm thick, h_r diverge from the d^{-2} asymptote starting at a $d \approx 30$ nm. This behavior is investigated more closely by plotting the near-field radiative heat transfer coefficient in Figs. 4(a) and 4(b) for the hypothetical cases $t_1 = t_3 = 1$ nm and $t_1 = t_3 = 0.1$ nm, respectively; in both figures, larger d values (from 20 nm up to 500 nm) are considered. It is worth noting that a near-field regime of thermal radiation cannot be readily defined for large gap d . Indeed, as d increases, the relative contribution from evanescent modes to the total radiative heat transfer decreases. We consequently fixed the limiting gap at 500 nm, keeping in mind that this value is an approximate threshold.

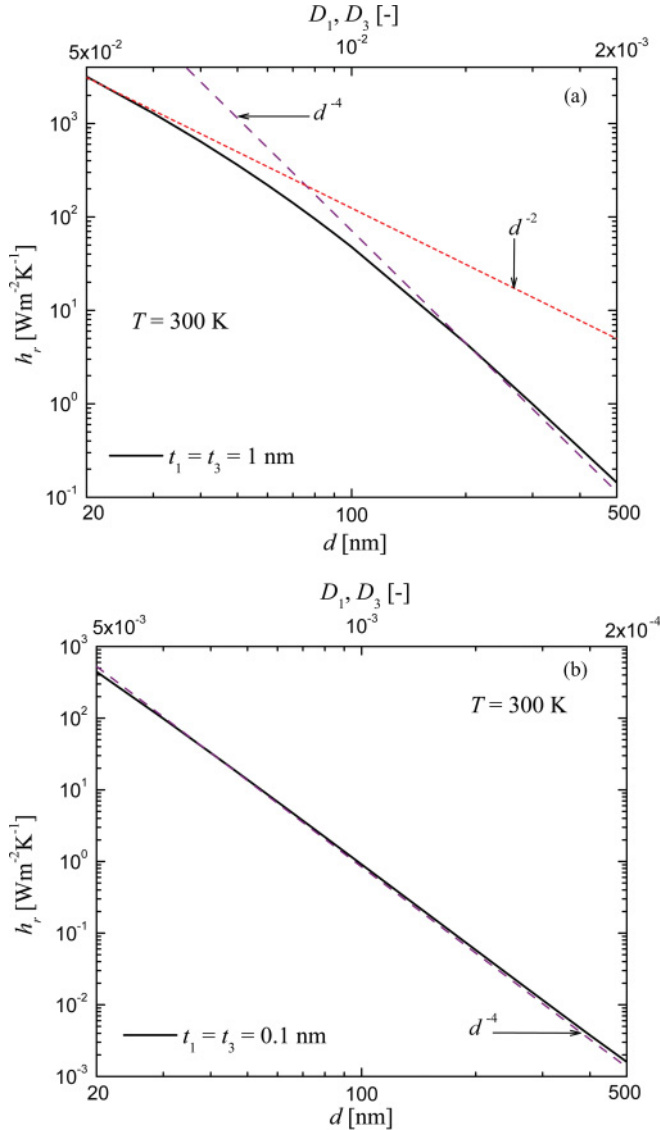


FIG. 4. (Color online) Radiative heat transfer coefficient h_r as a function of d : (a) Identification of the d^{-2} and d^{-4} regimes for $t_1 = t_3 = 1$ nm. (b) Identification of the d^{-4} regime for $t_1 = t_3 = 0.1$ nm. The temperature T for all simulations is fixed at 300 K.

Figure 4(a) shows that h_r follows a d^{-4} asymptote starting at $d \approx 200$ nm, where both D_1 and D_3 are 5×10^{-3} . The transition between the d^{-2} and d^{-4} regimes occurs between D values of about 3×10^{-2} and 5×10^{-3} . For the case in which $t_1 = t_3 = 0.1$ nm, Fig. 4(b) reveals that h_r varies as d^{-4} for the entire range of d considered. The case $t_1 = 1$ nm and $t_3 = 5$ nm was also analyzed, and it was observed that h_r varied as d^{-2} for d between 20 and 500 nm. Based on these results, the d^{-4} near-field thermal radiation regime emerges only when both layers are characterized by a D less than about 5×10^{-3} . Given this restriction, the d^{-4} regime appears to be purely theoretical, as it emerges when both films are of the order of a nanometer or less (keeping in mind that 500 nm is the maximum d). Also, such thin layers are likely to fall beyond the range of applicability of the macroscopic fluctuational electrodynamics; nevertheless, for the sake

of completeness, the d^{-4} regime is also analyzed in this paper.

The observations made in this section can be summarized as follows. When $D_1, D_3 \gg 1$, h_r varies as d^{-2} . A d^{-3} regime is achieved when $D_1 \ll 1$ and $D_3 \gg 1$ and vice versa. For $D_1, D_3 \ll 1$, h_r follows a d^{-2} power law; however, when both D_1 and D_3 are less than about 5×10^{-3} , h_r follows a d^{-4} asymptote.

IV. ASYMPTOTIC ANALYSIS OF THE NEAR-FIELD RADIATIVE HEAT TRANSFER COEFFICIENT

In this section, we analyze the coexistence of the d^{-2} , d^{-3} , and d^{-4} regimes via an asymptotic expansion of the near-field radiative transfer coefficient given by Eq. (2). As $d \rightarrow 0$, radiative heat transfer between nonmagnetic materials supporting SPhPs in the infrared is dominated by SPhPs, existing only in TM polarization, with $k_\rho \gg k_v$, where there is a large number of electromagnetic states in a very narrow spectral band. In the electrostatic limit where $k_\rho \gg k_v$, the z -component of the wave vector in medium j can be approximated as $k_{zj} \approx ik_\rho$, and the Fresnel reflection coefficients thus become independent of k_ρ ($r_{ij}^{TM} \approx (\epsilon_j - \epsilon_i)/(\epsilon_j + \epsilon_i)$). Using the dimensionless variable $\eta = k_\rho d$, the near-field radiative heat transfer coefficient between two layers can be approximated as follows:

$$h_r \approx \frac{1}{\pi^2 d^2} \int_0^\infty d\omega \frac{\partial \Theta(\omega, T)}{\partial T} \times \int_0^\infty \eta e^{-2\eta} d\eta \frac{\text{Im}(R_1^{TM}) \text{Im}(R_3^{TM})}{|1 - R_1^{TM} R_3^{TM} e^{-2\eta}|^2}, \quad (3)$$

where the lower limit of integration over η for evanescent modes has been approximated by 0 in the limit $d \rightarrow 0$.¹⁴ This approximation is justified as follows. The lower limit of integration for evanescent waves is $k_\rho = k_v$, which is, in terms of the dimensionless variable η , given by $\eta_v = k_v d$. For example, the magnitude of the wave vector in vacuum k_v ($=\omega/c_v$) at the resonant frequency of a single SiC-vacuum interface, $\omega_{\text{res}} \approx [(\omega_{TO}^2 + \epsilon_\infty \omega_{LO}^2)/(1 + \epsilon_\infty)]^{1/2} \approx 1.786 \times 10^{14}$ rad/s,¹⁶ is 5.957×10^5 rad/m. Assuming that the vacuum gap d is 10 nm thick, the dimensionless lower limit of integration over η becomes $\eta_v = 5.957 \times 10^{-3}$, such that it is justified to approximate the lower limit at 0. The film reflection coefficient in medium j , where $j = 1$ and 3, can also be written as $R_j^{TM} \approx r_{01}^{TM} (1 - e^{-2\eta D_j}) / (1 - (r_{01}^{TM})^2 e^{-2\eta D_j})$, where the fact that $r_{01}^{TM} = -r_{12}^{TM} = r_{23}^{TM} = -r_{34}^{TM}$ has been used and where $r_{01}^{TM} \approx (\epsilon_1 - 1)/(\epsilon_1 + 1)$.

As discussed in Sec. III, the emergence of a given near-field thermal radiation regime is function of the dimensionless ratios D_1 and D_3 . Hereafter, we analyze the limiting cases in which $D_1, D_3 \gg 1$, $D_1 \ll 1$ with $D_3 \gg 1$ (and vice versa) and $D_1, D_3 \ll 1$.

A. $D_1 \gg 1$ and $D_3 \gg 1$

When both t_1 and $t_3 \gg d$, D_1 and $D_3 \gg 1$, $R_1^{TM} \rightarrow r_{01}^{TM}$ and $R_3^{TM} \rightarrow r_{01}^{TM}$ such that Eq. (3) can be simplified as follows:

$$\begin{aligned} h_r &\approx \frac{1}{\pi^2 d^2} \int_0^\infty d\omega \frac{\partial \Theta(\omega, T)}{\partial T} [\text{Im}(r_{01}^{TM})]^2 \\ &\quad \times \int_0^\infty \eta e^{-2\eta} d\eta \frac{1}{|1 - (r_{01}^{TM})^2 e^{-2\eta}|^2} \\ &\sim \frac{1}{\pi^2 d^2} \int_0^\infty d\omega \frac{\partial \Theta(\omega, T)}{\partial T} [\text{Im}(r_{01}^{TM})]^2, \end{aligned} \quad (4)$$

where the integration over η is roughly approximated by unity around SPhP resonance, as done by Mulet *et al.*³ Equation (4) is the same as the expression obtained between two bulks, clearly showing that even if t_1 and $t_3 \ll \lambda_w$, the films behave as bulks with a h_r varying as d^{-2} provided that both t_1 and $t_3 \gg d$ (i.e., thick layers relative to the gap d). Note that a closed-form expression of the SPhP mediated radiative heat transfer coefficient between two planar half-spaces was derived recently by Rousseau *et al.*³⁰ The expression for h_r in Ref. 30 shows as in Eq. (4) that near-field radiative heat transfer follows a d^{-2} power law. In this paper, the approximation given by Eq. (4) is sufficient since we are interested by the variations of h_r as a function of d .

Physically, this result can be explained by analyzing the radiation penetration depth. In the electrostatic limit, the penetration depth of an evanescent wave in medium j , defined as $\delta_j = |k_{zj}|^{-1}$, can be approximated by $\delta \approx k_\rho^{-1}$. Then, we can argue that only evanescent waves with $\delta \geq d$ contribute to heat exchanges between media 1 and 3. Therefore, the largest contributing wave vector can be approximated as $k_{\rho, \max} \approx d^{-1}$ with an associated penetration depth $\delta_{\max} \approx d$. It can be shown that this largest contributing wave vector $k_{\rho, \max}$ dominates radiation heat transfer in the near-field where a large number of electromagnetic states is available in a narrow spectral band (see discussion in Ref. 9). Here, for D_1 and $D_3 \gg 1$, δ_{\max} is much smaller than the film thicknesses, such that SPhPs dominating radiant energy exchanges are absorbed by the layers very near the interfaces 1-2 and 2-3 (see Fig. 1). As discussed in Refs. 8 and 9, SPhPs are thermally excited at each film-vacuum interface depicted in Fig. 1, such that SPhP coupling within and between the films can occur. When $t_j \gg d$, dominant SPhPs with $k_{\rho, \max} \approx d^{-1}$ present at the interfaces 0-1 and 3-4 cannot contribute to radiant energy exchanges, and cannot couple with the dominant SPhPs at the interfaces 1-2 and 2-3; in other words, the interfaces 0-1 and 3-4 play a negligible role on the near-field radiative heat transfer. Consequently, the resonance of the radiative flux is located at ω_{res} of a single bulk-vacuum interface,⁹ and the two-film system is essentially behaving as two bulks. This conclusion is in line with the discussion provided by Basu and Zhang.³¹

B. $D_1 \ll 1$ and $D_3 \gg 1$ or $D_1 \gg 1$ and $D_3 \ll 1$

For the purpose of discussion, we set $t_1 \ll d$ and $t_3 \gg d$, keeping in mind that the inverse case will lead to the same conclusions. For this case, $R_1^{TM} \approx r_{01}^{TM}(1 - e^{-2\eta D_1})/(1 - (r_{01}^{TM})^2 e^{-2\eta D_1})$, while $R_3^{TM} \rightarrow r_{01}^{TM}$

such that Eq. (3) reduces to

$$\begin{aligned} h_r &\approx \frac{1}{\pi^2 d^2} \int_0^\infty d\omega \frac{\partial \Theta(\omega, T)}{\partial T} \text{Im}(r_{01}^{TM}) \\ &\quad \times \int_0^\infty \eta e^{-2\eta} d\eta \text{Im} \left(\frac{r_{01}^{TM}(1 - e^{-2\eta D_1})}{1 - (r_{01}^{TM})^2 e^{-2\eta D_1}} \right) \\ &\quad \times \frac{1}{\left| 1 - \frac{(r_{01}^{TM})^2(1 - e^{-2\eta D_1})e^{-2\eta}}{1 - (r_{01}^{TM})^2 e^{-2\eta D_1}} \right|^2}. \end{aligned} \quad (5)$$

When $D_1 \ll 1$, the term $\exp(-2\eta D_1)$ can be approximated as $1 - 2\eta D_1$ using a first-order Maclaurin series expansion, such that Eq. (5) can be written as follows:

$$\begin{aligned} h_r &\approx \frac{2D_1}{\pi^2 d^2} \int_0^\infty d\omega \frac{\partial \Theta(\omega, T)}{\partial T} \text{Im}(r_{01}^{TM}) \\ &\quad \times \int_0^\infty \eta^2 e^{-2\eta} d\eta \text{Im} \left[\frac{r_{01}^{TM}}{1 - (r_{01}^{TM})^2(1 - 2\eta D_1)} \right] \\ &\quad \times \left| \frac{1 - (r_{01}^{TM})^2(1 - 2\eta D_1)}{1 - (r_{01}^{TM})^2[1 - 2\eta D_1(1 - e^{-2\eta})]} \right|^2. \end{aligned} \quad (6)$$

As mentioned above, near-field radiative transfer is dominated by SPhPs with $k_{\rho, \max} \approx d^{-1}$, which implies that h_r is dominated by waves with $\eta_{\max} \approx 1$. At such a value of η , the term $1 - 2\eta D_1$ can be approximated as 1 since $D_1 \ll 1$, whereas the term $(1 - e^{-2\eta})$ is smaller than unity. Consequently, Eq. (6) can be rearranged as follows:

$$h_r \approx \frac{t_1}{2\pi^2 d^3} \int_0^\infty d\omega \frac{\partial \Theta(\omega, T)}{\partial T} \text{Im}(r_{01}^{TM}) \text{Im} \left(\frac{r_{01}^{TM}}{1 - (r_{01}^{TM})^2} \right), \quad (7)$$

where the integration over η gives $1/4$. The approximate expression for h_r is thus function of the thickness of the thinner layer only. The d^{-3} behavior obtained in Eq. (7), confirming the observations made in Sec. III, seems to be the signature of a resonance mismatch between the films, as explained hereafter.

First, let us consider film 1. SPhPs dominating thermal emission from that layer are characterized by $\delta_{\max} \gg t_1$ since $t_1 \ll d$. As a consequence, dominant SPhPs thermally generated at the interfaces 0-1 and 1-2 couple within layer 1, thus leading to a splitting of the emitted near-field spectrum incident on layer 3 into antisymmetric ω^+ and symmetric ω^- resonances. As D_1 decreases, the antisymmetric and symmetric resonant frequency bands approach, respectively, ω_{LO} and ω_{TO} . For film 3, SPhPs dominating the near-field thermal spectrum incident on medium 1 are characterized by $\delta_{\max} \ll t_3$ since $t_3 \gg d$, such that dominant SPhPs at the interfaces 2-3 and 3-4 do not couple within layer 3 (i.e., the interface 3-4 plays a negligible role in near-field radiative transfer), thus resulting into a single resonance at ω_{res} . Since spectral near-field emittance is the same as spectral near-field absorptance, the resonances of near-field thermal emission and absorption of layer 1 do not match the single resonance of near-field thermal emission and absorption of film 3. This mismatch between the spectral bands of high emission and absorption between layers 1 and 3 seems to manifest itself by a h_r varying as d^{-3} .

C. $D_1 \ll 1$ and $D_3 \ll 1$

The last case arises when both films are thinner than the gap d (D_1 and $D_3 \ll 1$). By substituting $R_1^{TM} \approx r_{01}^{TM}(1 - e^{-2\eta D_1})/(1 - (r_{01}^{TM})^2 e^{-2\eta D_1})$ and $R_3^{TM} \approx r_{01}^{TM}(1 - e^{-2\eta D_3})/(1 - (r_{01}^{TM})^2 e^{-2\eta D_3})$, the near-field radiative heat transfer coefficient given by Eq. (3) can thus be written as follows:

$$h_r \approx \frac{1}{\pi^2 d^2} \int_0^\infty d\omega \frac{\partial \Theta(\omega, T)}{\partial T} \times \int_0^\infty \eta e^{-2\eta} d\eta \operatorname{Im} \left(\frac{r_{01}^{TM}}{1 - (r_{01}^{TM})^2 (1 - 2\eta D_1)} \right) \times \operatorname{Im} \left(\frac{r_{01}^{TM}}{1 - (r_{01}^{TM})^2 (1 - 2\eta D_3)} \right) \times 4\eta^2 D_1 D_3 \frac{1}{\left| 1 - \frac{4\eta^2 D_1 D_3 (r_{01}^{TM})^2 e^{-2\eta}}{[1 - (r_{01}^{TM})^2 (1 - 2\eta D_1)][1 - (r_{01}^{TM})^2 (1 - 2\eta D_3)]} \right|^2}. \quad (8)$$

For D_1 and $D_3 \ll 1$, the resonances of near-field thermal emission and absorption for both films are split into antisymmetric ω^+ and symmetric ω^- modes. Indeed, SPhPs dominating near-field radiative heat transfer are characterized by $\delta_{\max} \gg t_1, t_3$ since $t_1, t_3 \ll d$. Therefore, SPhPs dominating near-field radiation transfer couple within the layers, and the four interfaces 0-1, 1-2, 2-3, and 3-4 play important roles.

Despite the fact that two resonances arise, most of the radiant energy is exchanged via the mode ω^- , approaching ω_{TO} for small D values, where the losses in the material are higher than for the ω^+ mode.⁹ At the transverse optical phonon frequency ω_{TO} , the real and imaginary parts of the dielectric function of a polar crystal modeled by a Lorentz oscillator are, respectively,

$$\varepsilon'_1 = \varepsilon_\infty \quad (9a)$$

and

$$\varepsilon''_1 = \frac{\varepsilon_\infty (\omega_{LO}^2 - \omega_{TO}^2)}{\Gamma \omega_{TO}}. \quad (9b)$$

In the electrostatic limit, the real and imaginary components of the Fresnel reflection coefficients in TM polarization are given respectively by

$$\operatorname{Re}(r_{01}^{TM}) \approx \frac{(\varepsilon'_1 - 1)(\varepsilon'_1 + 1) + (\varepsilon''_1)^2}{(\varepsilon'_1 + 1)^2 + (\varepsilon''_1)^2} \quad (10a)$$

and

$$\operatorname{Im}(r_{01}^{TM}) \approx \frac{2\varepsilon''_1}{(\varepsilon'_1 + 1)^2 + (\varepsilon''_1)^2}. \quad (10b)$$

For polar crystals such as SiC or cubic boron nitride (cBN),²⁷ the real and imaginary components of the dielectric function have orders of magnitude of 1 and 10^3 , respectively. Using Eqs. (10a) and (10b), it can be seen that $\operatorname{Re}((r_{01}^{TM})^2) = (\operatorname{Re}(r_{01}^{TM}))^2 - (\operatorname{Im}(r_{01}^{TM}))^2 \approx 1$, while $\operatorname{Im}((r_{01}^{TM})^2) = 2\operatorname{Re}(r_{01}^{TM})\operatorname{Im}(r_{01}^{TM}) \ll 1$. Therefore, if we assume as before that $1 - (r_{01}^{TM})^2(1 - 2\eta D_j) \approx 1 - (r_{01}^{TM})^2$

for $D_j \ll 1$, it can be seen that the denominator of Eq. (8) will take very small values.

To circumvent this problem, the term $(r_{01}^{TM})^2$ is expanded into its real and imaginary components as follows:¹⁴

$$1 - (r_{01}^{TM})^2(1 - 2\eta D_j) \approx 2\eta D_j - i\operatorname{Im}((r_{01}^{TM})^2)(1 - 2\eta D_j) \approx 2\eta D_j - i\operatorname{Im}((r_{01}^{TM})^2), \quad (11)$$

where the fact that $\operatorname{Re}((r_{01}^{TM})^2) \approx 1$ has been used. By assuming in the above expression that $2\eta D_j$ is the dominant term (i.e., $2\eta D_j > \operatorname{Im}((r_{01}^{TM})^2)$), it is possible to write that

$$\operatorname{Im} \left(\frac{r_{01}^{TM}}{1 - (r_{01}^{TM})^2 (1 - 2\eta D_1)} \right) \operatorname{Im} \left(\frac{r_{01}^{TM}}{1 - (r_{01}^{TM})^2 (1 - 2\eta D_3)} \right) \approx \frac{[\operatorname{Im}(r_{01}^{TM})]^2}{4\eta^2 D_1 D_3} \quad (12)$$

and

$$\frac{1}{\left| 1 - \frac{4\eta^2 D_1 D_3 (r_{01}^{TM})^2 e^{-2\eta}}{[1 - (r_{01}^{TM})^2 (1 - 2\eta D_1)][1 - (r_{01}^{TM})^2 (1 - 2\eta D_3)]} \right|^2} \approx \frac{1}{\left| 1 - (r_{01}^{TM})^2 e^{-2\eta} \right|^2} \approx 1. \quad (13)$$

Substitutions of Eqs. (12) and (13) into Eq. (8) leads to the following approximation for the near-field radiative heat transfer coefficient when D_1 and $D_3 \ll 1$, while $2\eta D_j > \operatorname{Im}((r_{01}^{TM})^2)$:

$$h_r \approx \frac{1}{4\pi^2 d^2} \int_0^\infty d\omega \frac{\partial \Theta(\omega, T)}{\partial T} [\operatorname{Im}(r_{01}^{TM})]^2, \quad (14)$$

where the integration over η gives $1/4$. Equation (14) shows that h_r varies as d^{-2} , thus confirming the trends observed in Sec. III. For the cases discussed previously, near-field radiative transfer was dominated by SPhPs with frequencies around ω_{res} ,⁹ where $\operatorname{Re}((r_{01}^{TM})^2) \approx 1$ and $\operatorname{Im}((r_{01}^{TM})^2) \ll 1$ were not applicable. This is why the extraneous operation of splitting $(r_{01}^{TM})^2$ into its real and imaginary components is done strictly for the case D_1 and $D_3 \ll 1$ where near-field radiation transfer occurs mostly around ω^- .

At $\omega = \omega_{TO}$, $\operatorname{Im}((r_{01}^{TM})^2)$ has an order of magnitude of 10^{-2} for materials such as SiC and cBN supporting SPhPs in the infrared (exact values of 7.3×10^{-3} and 8.9×10^{-3} , respectively, when using a Lorentz oscillator model). The approximation $2\eta D_j > \operatorname{Im}((r_{01}^{TM})^2)$ used to derived Eqs. (12) and (13) is consequently not applicable for D_j values smaller than $\operatorname{Im}((r_{01}^{TM})^2)$. This thus explains the results of Figs. 4(a) and 4(b) in which h_r diverged from the d^{-2} asymptote to reach a d^{-4} regime when both D_1 and D_3 were less than about 5×10^{-3} .

Assuming that $D_1, D_3 \ll 1$ and assuming that the term given in Eq. (11) is dominated by $\operatorname{Im}((r_{01}^{TM})^2)$ (i.e., $\operatorname{Im}((r_{01}^{TM})^2) > 2\eta D_j$), Eqs. (12) and (13) are modified as follows:

$$\operatorname{Im} \left(\frac{r_{01}^{TM}}{1 - (r_{01}^{TM})^2 (1 - 2\eta D_1)} \right) \operatorname{Im} \left(\frac{r_{01}^{TM}}{1 - (r_{01}^{TM})^2 (1 - 2\eta D_3)} \right) \approx \frac{1}{4[\operatorname{Im}(r_{01}^{TM})]^2} \quad (15)$$

and

$$\begin{aligned} & \left| 1 - \frac{4\eta^2 D_1 D_3 (r_{01}^{TM})^2 e^{-2\eta}}{[1 - (r_{01}^{TM})^2 (1 - 2\eta D_1)][1 - (r_{01}^{TM})^2 (1 - 2\eta D_3)]} \right|^2 \\ & \approx \frac{1}{\left| 1 + \frac{4\eta^2 D_1 D_3 \operatorname{Re}((r_{01}^{TM})^2) e^{-2\eta}}{[\operatorname{Im}((r_{01}^{TM})^2)]^2} + \frac{i4\eta^2 D_1 D_3 e^{-2\eta}}{[\operatorname{Im}((r_{01}^{TM})^2)]} \right|^2} \\ & \approx 1. \end{aligned} \quad (16)$$

Both the second and third terms in the denominator of Eq. (16) are much smaller than unity, since $\operatorname{Re}((r_{01}^{TM})^2) \approx 1$ and $D_1 D_3 \ll \operatorname{Im}((r_{01}^{TM})^2)$. Substitution of Eqs. (15) and (16) into Eq. (8) leads to the following approximation for the near-field radiative heat transfer coefficient when $D_1, D_3 \ll 1$ and $\operatorname{Im}((r_{01}^{TM})^2) > 2\eta D_j$:

$$h_r \approx \frac{3t_1 t_3}{8\pi^2 d^4} \int_0^\infty d\omega \frac{\partial \Theta(\omega, T)}{\partial T} \frac{1}{[\operatorname{Im}(r_{01}^{TM})]^2}, \quad (17)$$

where the integration over η gives $3/8$. Equation (17) confirms the conclusions stated in Sec. III: h_r follows a d^{-4} asymptote when both D_1 and D_3 have an order of magnitude of 10^{-3} or less. For this particular case only, h_r is a function of both film thicknesses t_1 and t_3 .

D. Regime map

The different near-field thermal radiation regimes arising between two layers supporting SPhPs in the infrared are illustrated in Fig. 5. This regime map summarizes the discussions of previous sections and constitutes the main result of this paper.

The regime map of Fig. 5 can be analyzed and interpreted as follows. For a given configuration with fixed layer thicknesses t_1 and t_3 , the near-field radiative heat transfer coefficient h_r follows a d^{-2} , d^{-3} , or a d^{-4} power law, depending on the values of D_1 and D_3 . Therefore, for a fixed set of t_1 and t_3 , variations of D_1 and D_3 are solely due to d . It is possible to visualize the different near-field radiation regimes involved for a given set of t_1 and t_3 as a function of d by plotting in Fig. 5 the ratio $D_3/D_1 = t_3/t_1$. The origin of this curve is determined by calculating D_1 and D_3 at the maximum possible d approximated earlier by 500 nm. Similarly, the end point is computed using a minimum d of 1 nm.

As observed in Sec. III, the fully developed d^{-2} , d^{-3} , and d^{-4} regimes are achievable only in the cases where $D_1, D_3 \gg 1$, $D_1, D_3 \ll 1$ and $D_1 \gg 1$ with $D_3 \ll 1$ (and vice versa). When these conditions are not met, h_r is in a transition zone (regions left blank in Fig. 5). We would like to emphasize here that these transition regions are not well defined, such that approximate thresholds were used to produce the regime map of Fig. 5 based on the results of Sec. III. We approximated that $D \gg 1$ above 2, while $D \ll 1$ below 0.5. It is also assumed that the transition from the d^{-2} to the d^{-4} regime occurs when both D_1 and D_3 are between 3×10^{-2} and 5×10^{-3} , while the fully developed d^{-4} regime is reached when $D_1, D_3 < 5 \times 10^{-3}$.

As illustrative examples, four different configurations are depicted in Fig. 5. The case where $t_1 = 50$ nm and $t_3 = 10$ nm, presented in Fig. 3(b), is depicted in the regime map, where it is clear that the transition region is connecting two fully developed d^{-2} regimes. In this transition zone, h_r is

lying around a d^{-3} asymptote, as observed in Fig. 3(b). For the extreme case in which both layers are 10 μm thick, thus behaving as bulks, h_r varies strictly as d^{-2} , as discussed previously in the literature.³ Clearly, the well-known d^{-2} regime of near-field thermal radiation between two planar half-spaces corresponds to the upper right corner of the regime map of Fig. 5.

The regime map is valid in the context of fluctuational electrodynamics where nonlocal effects are neglected. Given that and other limitations with regard to realistic layer thicknesses, it appears that the d^{-4} regime is a pure mathematical curiosity that falls beyond the range of applicability of the macroscopic fluctuational electrodynamics. The determination of the exact range of applicability of the regime map (in terms of smallest layer thicknesses and limiting separation gaps) is beyond the scope of this paper and would require further investigation of the impacts of spatial dispersion³² and of thermal emission beyond the fluctuational electrodynamics formalism³³ on near-field radiant energy exchange between two layers supporting SPhPs in the infrared.

V. CONCLUSIONS

We have studied near-field radiative heat transfer between two layers of thicknesses t_1 and t_3 supporting SPhPs in the infrared, where their separation distance (d) have been assumed to be much smaller than the dominant wavelength emitted (λ_w). By calculating the near-field radiative heat transfer coefficient h_r for silicon carbide and following an asymptotic analysis of h_r , we have shown the coexistence of d^{-2} , d^{-3} , and d^{-4} near-field thermal radiation regimes. It has also been demonstrated that these regimes cannot be solely defined using the layer thicknesses t_1 and t_3 , as done in the past.¹⁹ Indeed, near-field radiative heat transfer is also function of the penetration depth of the dominant SPhPs, which in turn is function of the gap thickness d . Consequently, $D_1 (=t_1/d)$ and $D_3 (=t_3/d)$ are the appropriate variables for determining near-field thermal radiation regimes.

When D_1 and $D_3 \gg 1$, SPhPs dominating radiation heat transfer in the near-field do not couple within the thin layers, and therefore the two layer system is essentially behaving as two bulks, where h_r varies as d^{-2} . For D_1 and $D_3 \ll 1$, dominant SPhPs couple within the films, resulting in a spectral distribution of radiative energy split in two modes. In that case, the spectral zones of high emission and absorption of layer 1 essentially match those of medium 3 (and vice versa). This leads to radiation heat transfer similar to the two bulk case, where h_r follows a d^{-2} power law. However, when both D_1 and D_3 are less than about 5×10^{-3} , h_r follows a d^{-4} asymptote. Due to the fact that near-field thermal radiation regimes can be defined up to a d value of about 500 nm, the d^{-4} behavior is observed theoretically when the thickness of the films is of the order of a nanometer or less. Such thin layers are likely to fall beyond the range of applicability of the macroscopic fluctuational electrodynamics employed in this study. Moreover, even if fluctuational electrodynamics was applicable for such thin layers, this d^{-4} regime is not likely to be observable experimentally due to the extremely small film thicknesses. For $D_1 \ll 1$ and $D_3 \gg 1$, dominant SPhPs couple within layer 1, while such an interaction between the

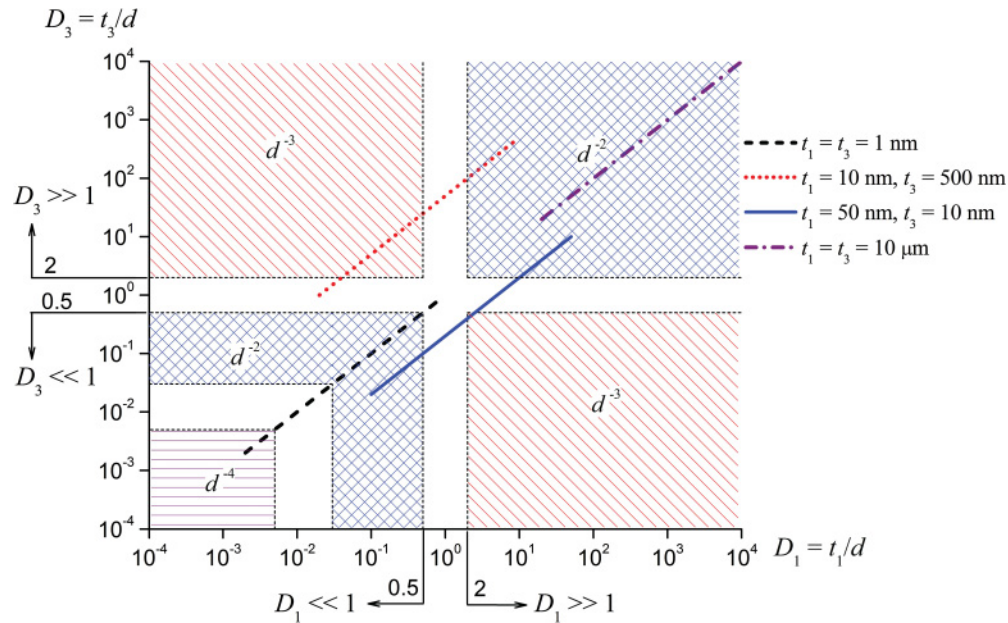


FIG. 5. (Color online) Regime map of near-field thermal radiation between two layers supporting SPhPs in the infrared. The map is applicable in the extreme near-field where $d \ll \lambda_w$.

dominant SPhPs is impossible in film 3 (vice versa for $D_1 \gg 1$ and $D_3 \ll 1$). As a consequence, an important mismatch between the spectral bands of high emission and absorption of media 1 and 3 is induced, thus leading to a h_r varying as d^{-3} .

The analysis presented in this paper, summarized in a regime map, provides physical insights on near-field radiative transfer between layers supporting SPhPs in the infrared. As a future research effort, it would be interesting to determine exactly the range of applicability of these near-field thermal radiation regimes by determining a minimal thickness for the

films as well as limiting values of the gap separating the two layers. The development of a near-field thermal radiation regime map for coated materials would also be valuable from a practical point of view.

ACKNOWLEDGMENTS

This work is partially supported by a FP-7-PEOPLE-IRG-2008 (Grant No: 239382 NF-RAD) to MPM at Ozyegin University in Istanbul.

*Corresponding author: mfrancoeur@mech.utah.edu

¹D. Polder and M. Van Hove, *Phys. Rev. B* **4**, 3303 (1971).

²J. J. Loomis and H. J. Maris *Phys. Rev. B* **50**, 18517 (1994).

³J.-P. Mulet, K. Joulain, R. Carminati, and J.-J. Greffet, *Microscale Thermophys. Eng.* **6**, 209 (2002).

⁴I. Dorofeyev, J. Jersch, and H. Fuchs, *Ann. Phys. (Leipzig)* **12**, 421 (2003).

⁵K. Joulain, J.-P. Mulet, F. Marquier, R. Carminati, and J.-J. Greffet, *Surf. Sci. Rep.* **57**, 59 (2005).

⁶A. I. Volokitin and B. N. J. Persson, *Rev. Mod. Phys.* **79**, 1291 (2007).

⁷S. Basu, Z. M. Zhang, and C. J. Fu, *Int. J. Energy Res.* **33**, 1203 (2009).

⁸M. Francoeur, M. P. Mengüç and R. Vaillon, *J. Appl. Phys.* **107**, 034313 (2010).

⁹M. Francoeur, M. P. Mengüç and R. Vaillon, *J. Phys. D* **43**, 075501 (2010).

¹⁰M. Francoeur, M. P. Mengüç, and R. Vaillon, *Appl. Phys. A Mater.* **103**, 547 (2011).

¹¹L. Hu, A. Narayanaswamy, X. Chen, and G. Chen, *Appl. Phys. Lett.* **92**, 133106 (2008).

¹²S. Shen, A. Narayanaswamy, and G. Chen, *Nano Lett.* **9**, 2909 (2009).

¹³E. Rousseau, A. Siria, G. Jourdan, S. Volz, F. Comin, J. Chevrier, and J.-J. Greffet, *Nat. Photonics* **3**, 514 (2009).

¹⁴S.-A. Biehs, D. Reddig, and M. Holthaus, *Eur. Phys. J. B* **55**, 237 (2007).

¹⁵S.-A. Biehs, *Eur. Phys. J. B* **58**, 423 (2007).

¹⁶M. Francoeur, M. P. Mengüç, and R. Vaillon, *Appl. Phys. Lett.* **93**, 043109 (2008).

¹⁷C. J. Fu and W. C. Tan, *J. Quant. Spectrosc. Radiat. Transfer* **110**, 1027 (2009).

¹⁸P. Ben-Abdallah, K. Joulain, J. Drevillon, and G. Domingues, *Appl. Phys. Lett.* **94**, 153117 (2009).

¹⁹P. Ben-Abdallah, K. Joulain, J. Drevillon, and G. Domingues, *J. Appl. Phys.* **106**, 044306 (2009).

²⁰P. Ben-Abdallah, K. Joulain, and A. Pryamikov, *Appl. Phys. Lett.* **96**, 143117 (2010).

- ²¹R. S. DiMatteo, P. Greiff, S. L. Finberg, K. A. Young-Waithe, H. K. H. Choy, M. M. Masaki, and C. G. Fonstad, *Appl. Phys. Lett.* **79**, 1894 (2001).
- ²²M. D. Whale and E. G. Cravalho, *IEEE Trans. Energy Conversion* **17**, 130 (2002).
- ²³M. Laroche, R. Carminati, and J.-J. Greffet, *J. Appl. Phys.* **100**, 063704 (2006).
- ²⁴K. Park, S. Basu, W. P. King, and Z. M. Zhang, *J. Quant. Spectrosc. Radiat. Transfer* **109**, 305 (2008).
- ²⁵M. Francoeur, R. Vaillon, and M. P. Mengüç, *IEEE Trans. Energy Conversion* **26**, 686 (2011).
- ²⁶S. M. Rytov, Y. A. Kravtsov, and V. I. Tatarski, *Principles of Statistical Radiophysics* (Springer, New York, 1989), Vol. 3, pp. 109–173.
- ²⁷M. Francoeur, M. P. Mengüç, and R. Vaillon, *J. Quant. Spectrosc. Radiat. Transfer* **110**, 2002 (2009).
- ²⁸E. Rousseau, M. Laroche, and J.-J. Greffet, *Appl. Phys. Lett.* **95**, 231913 (2009).
- ²⁹E. D. Palik *Handbook of Optical Constants of Solids* (Academic Press, San Diego 1998), Vol. 1, pp. 587–596.
- ³⁰E. Rousseau, M. Laroche, and J.-J. Greffet, hal-00428574, [<http://hal.archives-ouvertes.fr/hal-00428574/fr/>] (Access date July 11, 2011).
- ³¹S. Basu and Z. M. Zhang, *Appl. Phys. Lett.* **95**, 133104 (2009).
- ³²P.-O. Chapuis, S. Volz, C. Henkel, K. Joulain, and J.-J. Greffet, *Phys. Rev. B* **77**, 035431 (2008).
- ³³A. Perez-Madrid, L. C. Lapas, and J. M. Rubi, *Phys. Rev. Lett.* **103**, 048301 (2009).